Evaluation of numerical stress-point algorithms on elastic–plastic models for unsaturated soils with hardening dependent on the degree of saturation

F. Cattaneo [a], G. Della Vecchia [b], C. Jommi [c,*]

[a] Universitá degli Studi di Brescia, Via Branze 38, 25121 Brescia, Italy
[b] Politecnico di Milano, Piazza Leonardo da Vinci 32, 20133 Milano, Italy
[c] Delft University of Technology, P.O. Box 5048, 2600 GA Delft, The Netherlands

1. Introduction

In the last years the capability of predicting the behaviour of unsaturated soils has been improved significantly, thanks to the development of enhanced hydro-mechanical constitutive laws able to account for strongly coupled non-linear and irreversible features. Local integration of the constitutive laws, named stress point algorithm, is a key component for successful implementation of these models in numerical codes for the solution of engineering problems. As the stress state is updated at each Gauss point several times during the analysis, the stress point algorithm must be accurate, robust and efficient in order not to undermine the results of numerical approaches.

In the context of the most common formulation of coupled finite element analysis, the integration is carried out at the Gauss point level given the strain increment, directly calculated from the displacement field, and the liquid and gas pressure increments.

Alternative strategies may be pursued for the integration of stress paths involving irreversible and non-linear changes of mechanical and hydraulic conditions. Explicit integration schemes may prove to be a valuable choice during the model development stage, as they generally do not require heavy analytical effort. Adaptive substepping procedures are invoked to guarantee accuracy and error control when they are adopted in finite element analysis. Explicit schemes with adaptive subincrementation refer mostly to the works of Sloan [1] and Sloan et al. [2]. Explicit methods applied to unsaturated soils have been firstly discussed by Sheng et al. [3,4], with emphasis on automatic substepping, and Sheng et al. [5]. Numerical strategies for explicit algorithms to deal with non-convexity of the yield surface at the transition between saturated and unsaturated states have been tackled by Sheng et al. [6]. Sanchez et al. [7] have proposed a multi-mechanism generalisation of Sloan's integration scheme for generalised plasticity laws in the implementation of a double structure model for expansive clays. With reference to the Barcelona Basic Model (BBM) and related constitutive models, Solowski and Gallipoli [8,9] have studied in detail several Runge–Kutta methods, with particular attention on efficiency and accuracy issues, and proposed a novel explicit integration scheme based on Richardson interpolation. Application of

drift reduction procedures to the latter explicit stress point algorithm has been proposed by Solowski et al. [10].

In view of the application of hydro-mechanical models to real scale problems, implicit algorithms are usually preferred, due to their higher efficiency. Implicit methods for unsaturated soil models have been discussed by Vaunat et al. [11], Zhang et al. [12], Hoyos and Arduino [13], Zhang and Zhou [14] and Tamagnini and De Gennaro [15].

Comparisons between refined explicit algorithms and implicit ones have been discussed by Potts and Ganendra [16] and Abbo and Sloan [17] on models for saturated soils. For unsaturated soils a similar comparison has been presented by Hofmann et al. [18], with reference to the BBM or similar models, in which the constitutive equations are written as a function of net stress $\boldsymbol{\sigma} - u_g\boldsymbol{\delta}$ and suction $u_g - u_l$, being $\boldsymbol{\sigma}$ the Cauchy stress tensor, $\boldsymbol{\delta}$ the Kronecker identity second order tensor, u_g and u_l the gas and the liquid pressure, respectively. More recently, Gonzalez and Gens [19] have examined the numerical performance of integration algorithms also for models that take into account the degree of saturation in the constitutive stress definition.

Several models characterised by different choices in terms of constitutive variables, i.e. stress variables linked to the elastic strain [20], have been presented in the literature. Inherent hydromechanical coupling of the unsaturated behaviour is the main reason which justified the introduction of constitutive stresses including the degree of saturation Sr in the formulation of constitutive models. In recent years, various authors adopted the so-called average skeleton stress [21]

$$\hat{\boldsymbol{\sigma}} = (\boldsymbol{\sigma} - u_g\boldsymbol{\delta}) + Sr(u_g - u_l)\boldsymbol{\delta} \qquad (1)$$

as constitutive stress. This choice, together with a retention model dependent on void ratio, allows some aspects of hydro-mechanical multi-phase coupling to be already embedded in the formulation.

In this paper the performance of an explicit and an implicit algorithm are discussed with reference to the latter class of constitutive models. Convergence and accuracy are analysed along different hydro-mechanical paths for both algorithms. Numerical simulations performed with the explicit algorithm are evaluated in terms of normalised incremental work, which proves to be a measure of the potential difficulties which the algorithm can suffer.

2. Elastic–plastic constitutive formulation

To describe the soil response in unsaturated conditions, both hydraulic and mechanical constitutive relationship must be introduced. The hydraulic constitutive law, named water retention curve, describes the dependence of the amount of water stored in the soil pores as a function of suction. Limiting the attention to a wide class of models relating the quantity of water in the pore space, expressed for example in terms of water ratio e_w (i.e. the ratio between the volume of water and the volume of solids), to the suction s and to the void ratio e, the retention curve can be described in the general form

$$e_w = e_w(s, e). \qquad (2)$$

For this class of retention models, the variation of water content and of degree of saturation in the incremental step depend directly on the suction increment and on the total volumetric strain increment. Being uncoupled from the plastic strain increment, the variation of degree of saturation can be calculated a priori by a suitable integration method, before entering the mechanical constitutive routine. Therefore, at the beginning of the latter numerical integration procedure, the total strain increment, the suction increment, and the degree of saturation increment are known. The unknowns are the updated constitutive stress and the updated plastic variables.

As for the mechanical part of the constitutive model, elastoplasticity with generalised hardening provides a suitable framework for the stress–strain behaviour of unsaturated soils. Under the hypothesis of small strain, the strain rate is decomposed additively in an elastic, reversible, part, $\dot{\boldsymbol{\varepsilon}}^e$, and a plastic, irreversible, one, $\dot{\boldsymbol{\varepsilon}}^p$:

$$\dot{\boldsymbol{\varepsilon}} = \dot{\boldsymbol{\varepsilon}}^e + \dot{\boldsymbol{\varepsilon}}^p. \qquad (3)$$

The elasticity tensor $\mathbf{D}^e$ links the constitutive stress rate to the elastic strain rate:

$$\dot{\hat{\boldsymbol{\sigma}}} = \mathbf{D}^e\dot{\boldsymbol{\varepsilon}}^e = \mathbf{D}^e(\dot{\boldsymbol{\varepsilon}} - \dot{\boldsymbol{\varepsilon}}^p). \qquad (4)$$

In the following, the behaviour of the material inside the yield locus is assumed to be hyperelastic, so that the relationship between $\boldsymbol{\varepsilon}^e$ and $\dot{\hat{\boldsymbol{\sigma}}}$ is bijective. To complete the description of the actual state of the unsaturated soil, a vector of internal variables $\mathbf{q}$ is introduced, describing the effect of strain history, in terms of plastic strain $\boldsymbol{\varepsilon}^p$, and of coupled variables on material response. Without loss of generality, models adopting the degree of saturation, Sr, as hardening variable are discussed henceforth. For any admissible value of $\mathbf{q}$, the stress state $\hat{\boldsymbol{\sigma}}$ is constrained to belong to the convex set E_σ

$$E_\sigma = \{(\hat{\boldsymbol{\sigma}}, \mathbf{q}) | f(\hat{\boldsymbol{\sigma}}, \mathbf{q}) \leqslant 0\}, \qquad (5)$$

where f is the yield function. The boundary of the set E_σ is called yield surface, while its internal part is the elastic domain.

For the class of models investigated in this paper, the evolution of plastic strain is defined prescribing the flow rule

$$\dot{\boldsymbol{\varepsilon}}^p = \dot{\lambda}\mathbf{Q} \qquad \mathbf{Q} := \frac{\partial g}{\partial \boldsymbol{\sigma}}, \qquad (6)$$

where g is the plastic potential, and $\dot{\lambda}$ a non-negative scalar named plastic multiplier.

The evolution of the internal variables $\mathbf{q}$ is provided by a generalised hardening law of the following type:

$$\dot{\mathbf{q}} = \dot{\lambda}\mathbf{h}(\hat{\boldsymbol{\sigma}}, \mathbf{q}, Sr) + \dot{Sr}\boldsymbol{\eta}(\hat{\boldsymbol{\sigma}}, \mathbf{q}, Sr) \qquad (7)$$

where $\mathbf{h}$ and $\boldsymbol{\eta}$ are the so-called hardening functions. The first term describes the changes in the internal variables associated with plastic strains, while the second term describes a reversible evolution of the elastic locus with the hydraulic history, ruled by changes in the degree of saturation.

The plastic multiplier $\dot{\lambda}$ is subjected to the Kuhn–Tucker conditions:

$$\dot{\lambda} \geqslant 0, \qquad f(\hat{\boldsymbol{\sigma}}, \mathbf{q}) \leqslant 0, \qquad \dot{\lambda}f(\hat{\boldsymbol{\sigma}}, \mathbf{q}) = 0, \qquad (8)$$

stating that plastic strains may occur only for states on the yield surface, and to the consistency condition

$$\dot{\lambda}\dot{f} = 0, \qquad (9)$$

which forces the state of the material to remain on the yield surface during plastic loading. Let

$$\mathbf{P} = \frac{\partial f}{\partial \boldsymbol{\sigma}} \quad \mathbf{W} = \frac{\partial f}{\partial \mathbf{q}} \qquad (10)$$

denote the gradients of f with respect to $\boldsymbol{\sigma}$ and $\mathbf{q}$. From the consistency condition (9), the elastic law (4) and the flow rule (6), the following expression for the plastic multiplier in terms of $\dot{\boldsymbol{\varepsilon}}$ and $\dot{Sr}$ is obtained:

$$\dot{\lambda} = \frac{1}{K_p}(\mathbf{P} \cdot \mathbf{D}^e\dot{\boldsymbol{\varepsilon}} + \mathbf{W} \cdot \boldsymbol{\eta}\dot{Sr}), \qquad (11)$$

provided that:

$$K_p = \mathbf{P} \cdot \mathbf{D}^e\mathbf{Q} - \mathbf{W} \cdot \mathbf{h} > 0. \qquad (12)$$

3. Stress point algorithms

The total load path is divided initially in a number of time steps of size Δt_i. Let Δt_{n+1} be the time step bounded by t_n and t_{n+1}. The state of the material $(\hat{\boldsymbol{\sigma}}_n, \mathbf{q}_n, \boldsymbol{\varepsilon}_n, \boldsymbol{\varepsilon}_n^p, Sr_n)$ is assumed to be completely known at time t_n. Within the common framework for finite element analysis involving unsaturated soils, the unknowns $\hat{\boldsymbol{\sigma}}_{n+1}, \mathbf{q}_{n+1}$ and $\boldsymbol{\varepsilon}_{n+1}^p$ are determined from the respective values at time t_n and from given increments $\Delta\boldsymbol{\varepsilon}$, Δu_l and Δu_g. As pointed out before, for the class of retention models considered, the increment of water ratio Δe_w and of degree of saturation ΔSr in the time step can be calculated before entering the mechanical constitutive law routine:

$$e_w^{n+1} = e_w(e_w^n, \Delta u_g, \Delta u_l, \Delta\boldsymbol{\varepsilon}) \, Sr^{n+1} = Sr(Sr^n, \Delta u_g, \Delta u_l, \Delta\boldsymbol{\varepsilon})$$

$$\Delta e_w = e_w^{n+1} - e_w^n \, \Delta Sr = Sr^{n+1} - Sr^n.$$

Therefore, at the beginning of the stress point algorithm routine, all the previous quantities are known.

The most common approaches for the integration of the elasto-plastic constitutive Eqs. (4)–(8) can be summarised as:

- explicit methods (e.g. Refs. [1,2,22]);
- implicit (backward Euler) methods (e.g. Refs. [23–25]);
- θ-methods (e.g. Ref. [26]).

A refined explicit algorithm of the Runge–Kutta family [1] and a fully implicit backward Euler scheme [23] were implemented in a constitutive driver, able to tackle any stress path under general mixed static and kinematic control conditions [27], to evaluate their performance along strongly coupled hydro-mechanical paths.

3.1. Explicit method

The elastic trial solution is obtained by means of an explicit procedure. Afterwards the Kuhn–Tucker conditions are checked. If the latter are violated a plastic integration step is performed.

3.1.1. Elastic predictor
Assuming that the step is completely elastic, the trial state, obtained by freezing the plastic flow (i.e. $\dot{\lambda}^{trial} = 0$), is calculated with an explicit approach:

$$\hat{\boldsymbol{\sigma}}_{n+1}^{trial} = \hat{\boldsymbol{\sigma}}_n + \Delta\hat{\boldsymbol{\sigma}}_{n+1}^{trial} = \hat{\boldsymbol{\sigma}}_n + \mathbf{D}^e(\hat{\boldsymbol{\sigma}}_n)\Delta\boldsymbol{\varepsilon} \tag{14a}$$

$$\mathbf{q}_{n+1}^{trial} = \mathbf{q}_n + \Delta Sr\,\boldsymbol{\eta}(\hat{\boldsymbol{\sigma}}_n, \mathbf{q}_n, Sr_n). \tag{14b}$$

The trial elastic solution is checked against a trial yield surface, which might be different from the initial one, due to the updating of the internal variables for degree of saturation changes. If $f_{n+1}^{trial} = f(\hat{\boldsymbol{\sigma}}_{n+1}^{trial}, \mathbf{q}_{n+1}^{trial}) \leqslant 0$, the trial state satisfies the Kuhn–Tucker conditions (8) and it coincides with the converged solution in the step. Otherwise, if $f_{n+1}^{trial} > 0$, a plastic integration step must be performed.

3.1.2. Intersection with yield surface
This step is necessary if the initial stress state is strictly inside the yield locus, i.e. $f_n < 0$, and the intersection with the trial yield surface must be found before starting the plastic integration step. The problem of finding the stress and the internal variables at the yield surface intersection is equivalent to the determination of the scalar quantity α which satisfies the equation

$$f(\hat{\boldsymbol{\sigma}}_n + \alpha\mathbf{D}^e\Delta\boldsymbol{\varepsilon}, \mathbf{q}_n + \alpha\Delta Sr\boldsymbol{\eta}) = 0. \tag{15}$$

The increment of degree of saturation is treated as an additional strain component and the same value of α is adopted for both increments.

To highlight the role of the increment of degree of saturation in the intersection of the stress path with the yield surface, it is useful to consider a hypothetical case involving null strain increment. An increment in the degree of saturation reduces the size of the yield surface, so that the initial stress state may fall outside (Fig. 1) the updated trial yield surface. In this case, the value of α must be found which satisfies:

$$f(\hat{\boldsymbol{\sigma}}_n, \mathbf{q}_n + \alpha\Delta Sr\boldsymbol{\eta}) = 0. \tag{16}$$

Until the yield surface reaches the stress state no plastic strain will occur.

In general, Eq. (15) is non-linear with respect to the variable α and can be solved by a variety of numerical methods, e.g. bisection, Regula-Falsi, secant and Newton–Raphson. As α is bounded in the interval $0 - 1$, Regula Falsi procedure proves to be a valuable choice [28].

3.1.3. Plastic integration step
Stress and internal variables on the yield surface become the initial values at the beginning of the plastic integration step, which consists in solving the non-linear system of ordinary differential Eqs. (4) and (7). The strain and degree of saturation increments to consider in this step are:

$$\Delta\boldsymbol{\varepsilon}^{ep} = (1 - \alpha)\Delta\boldsymbol{\varepsilon} \tag{17a}$$

$$\Delta Sr^{ep} = (1 - \alpha)\Delta Sr, \tag{17b}$$

where ΔSr^{ep} is that part of degree of saturation change which contributes to irreversible strain.

Several methods have been proposed to integrate the non-linear constitutive laws. All of them require a sub-stepping procedure, to limit the integration error. Among them, the algorithms belonging to the Runge–Kutta's class, with automatic substepping and error control, have proven to be reliable and efficient [2]. With this class of algorithms the substep size is adapted to modify the substep size by comparing two different order estimates of the solution. The Runge–Kutta–Dormand–Prince algorithm was chosen here.

The following procedure was implemented to integrate the plastic step:

1. Set the step initial pseudo-time to $T = \frac{t - t_n}{t_{n+1} - t_n} = 0$.
2. Set the pseudo-time increment to $\Delta T = 1 - T$.
3. For each level i (with i ranging from 1 to p, where p is the order of the Runge–Kutta method used):
   (a) compute

$$\hat{\boldsymbol{\sigma}}^i = \hat{\boldsymbol{\sigma}}_n + \sum_{k=0}^{i-1}\beta_{ik}\Delta\hat{\boldsymbol{\sigma}}^k \, \mathbf{q}^i = \mathbf{q}_n + \sum_{k=0}^{i-1}\beta_{ik}\Delta\mathbf{q}^k.$$
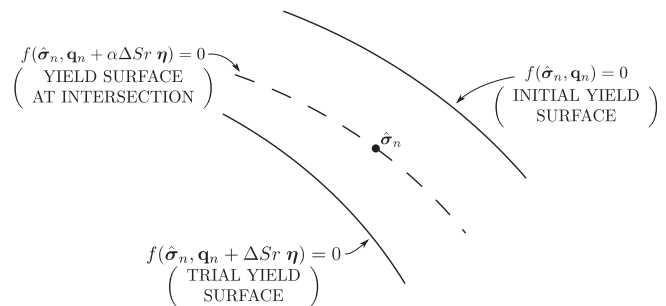

Fig. 1. Intersection due to degree of saturation.

(b) Compute the plastic multiplier

$$\Delta\lambda^{i+1} = \frac{1}{K_p}(\mathbf{P} \cdot \mathbf{D}^e \Delta T \Delta \boldsymbol{\varepsilon}^{ep} + \mathbf{W}\boldsymbol{\eta}\Delta T \Delta Sr^{ep})$$

with

$$K_p = \mathbf{P} \cdot \mathbf{D}^e \Delta T \mathbf{Q} - \mathbf{W}\mathbf{h},$$

where $\mathbf{P}$, $\mathbf{D}^e$, $\mathbf{W}$, $\boldsymbol{\eta}$ and $\mathbf{h}$ are evaluated using $\hat{\boldsymbol{\sigma}}^i$ and $\mathbf{q}^i$.

(c) Compute the stress and internal variables increments

$$\Delta\hat{\boldsymbol{\sigma}}^{i+1} = \mathbf{D}^e(\Delta T \Delta \boldsymbol{\varepsilon}^{ep} - \Delta\lambda^{i+1}\mathbf{Q}) \tag{18}$$

$$\Delta\mathbf{q}^{n+1} = \Delta\lambda^{i+1}\mathbf{h} + \Delta T \Delta Sr^{ep}\boldsymbol{\eta}. \tag{19}$$

4. Calculate stresses and internal variables for the two Runge–Kutta methods (denoted by the superscript $\sim$ for order p and $-$ for order $p - 1$):

$$\tilde{\hat{\boldsymbol{\sigma}}}_{n+1} = \hat{\boldsymbol{\sigma}}_n + c_i\Delta\hat{\boldsymbol{\sigma}}^i \qquad \bar{\hat{\boldsymbol{\sigma}}}_{n+1} = \hat{\boldsymbol{\sigma}}_n + \bar{c}_i\Delta\hat{\boldsymbol{\sigma}}^i$$

$$\tilde{\mathbf{q}}_{n+1} = \mathbf{q}_n + c_i\Delta\mathbf{q}^i \qquad \bar{\mathbf{q}}_{n+1} = \mathbf{q}_n + \bar{c}_i\Delta\mathbf{q}^i.$$

5. Determine the relative error for the current substep:

$$\xi = \max_j \left(\frac{\|\tilde{\hat{\boldsymbol{\sigma}}}_{n+1} - \bar{\hat{\boldsymbol{\sigma}}}_{n+1}\|}{\|\tilde{\hat{\boldsymbol{\sigma}}}_{n+1}\|}, \frac{|\tilde{q}^j_{n+1} - \bar{q}^j_{n+1}|}{|\tilde{q}^j_{n+1}|} \right). \tag{20}$$

6. If $\xi > TOL$, the substep must be reduced and a smaller pseudo-time increment has to be set

$$\Delta T = \Delta T \cdot 0.9 \left(\frac{\xi}{TOL}\right)^{1/p}, \tag{21}$$

then going back to step 3. The value 0.9 was assumed according to Sheng et al. [3].

7. If $\xi \leqslant TOL$, the substep is acceptable, and stresses, internal variables, degree of saturation and pseudo-time are updated:

$$\hat{\boldsymbol{\sigma}}_{n+1} = \tilde{\hat{\boldsymbol{\sigma}}}_{n+1} \quad \mathbf{q}_{n+1} = \tilde{\mathbf{q}}_{n+1} \quad Sr_{n+1} = Sr_n + \Delta T \Delta Sr^{ep} \quad T = T + \Delta T.$$

8. Check for pseudo-time T. If T is equal to 1, plastic step is completed. Otherwise, the remaining part must be still integrated following the same procedure as before starting from point 2.

9. Check for the stress state to lie on the yield surface. If not, a yield surface drift correction is necessary.

Table 1 reports the Butcher's matrix for the coefficients used by the Runge–Kutta–Dormand–Prince method.

3.1.4. Correction for yield surface drift

When an explicit algorithm is adopted, the plastic extension does not force the stress state to lie on the yield surface. The constraint $f_{n+1} = 0$ has to be checked at the end of the plastic step and, in case it was violated, consistency must be restored. Explicit stress integration methods with reduced drift for the BBM class of models have been recently proposed in the literature [10]. Here, for the class of models investigated in the following, the classical method proposed by Sloan [1] and Jakobsen and Lade [22] was adopted.

Table 1
Butcher's matrix for Runge–Kutta–Dormand–Prince method [2].

k	β_{k0}	β_{k1}	β_{k2}	β_{k3}	β_{k4}	c_k	$\bar{c}_k$
0	–	–	–	–	–	$\frac{31}{540}$	$\frac{19}{216}$
1	$\frac{1}{5}$	–	–	–	–	0	0
2	$\frac{3}{40}$	$\frac{9}{40}$	–	–	–	$\frac{190}{297}$	$\frac{1000}{2079}$
3	$\frac{3}{10}$	$-\frac{9}{10}$	$\frac{6}{5}$	–	–	$-\frac{145}{108}$	$-\frac{125}{216}$
4	$\frac{226}{72}$	$-\frac{25}{27}$	$\frac{880}{729}$	$\frac{55}{729}$	–	$\frac{351}{220}$	$\frac{81}{88}$
5	$-\frac{181}{270}$	$\frac{5}{2}$	$-\frac{266}{297}$	$-\frac{91}{27}$	$\frac{189}{55}$	$\frac{1}{20}$	$\frac{5}{56}$

Assuming that the internal variables $\mathbf{q}_{n+1}$ remain constant during the correction, the stress state is modified in order to restore the consistency condition. A scalar β must be found, so that

$$f(\hat{\boldsymbol{\sigma}}^*_{n+1}, \mathbf{q}_{n+1}) = 0, \qquad \hat{\boldsymbol{\sigma}}^*_{n+1} = \hat{\boldsymbol{\sigma}}_{n+1} + \beta\frac{\partial g}{\partial\hat{\boldsymbol{\sigma}}}\Big|_{n+1}, \tag{22}$$

where $\hat{\boldsymbol{\sigma}}_{n+1}$ is the stress state at the end of the explicit integration procedure, and $\hat{\boldsymbol{\sigma}}^*_{n+1}$ is the final corrected stress state, satisfying the consistency condition, for the given internal variables. Eq. (22) define a single non-linear equation of the form $F(\beta) = 0$, that must be solved iteratively, for instance by a Newton–Raphson algorithm.

3.2. Implicit method

Following [24], the classical elastic–plastic operator split [23] of the original problem (OR) may be extended to generalised hardening rules, dependent on both plastic strains and degree of saturation, as the sum of an elastic predictor (EP) and a plastic corrector (PC):

OR	=	EP	+	PC
$\dot{\boldsymbol{\varepsilon}}^e = \dot{\boldsymbol{\varepsilon}} - \lambda\mathbf{Q}$		$\dot{\boldsymbol{\varepsilon}}^e = \dot{\boldsymbol{\varepsilon}}$		$\dot{\boldsymbol{\varepsilon}}^e = -\lambda\mathbf{Q}$
$\dot{\mathbf{q}} = \lambda\mathbf{h} + \dot{S}r\boldsymbol{\eta}$		$\dot{\mathbf{q}} = \dot{S}r\boldsymbol{\eta}$		$\dot{\mathbf{q}} = \lambda\mathbf{h}$

As in the case of the explicit scheme, the elastic predictor problem is solved and a trial elastic state is obtained. Then, the constraint $f^{trial} \leqslant 0$ is checked, and if it is violated, the trial state is taken as the initial condition for the plastic corrector problem. Otherwise the trial state coincides with the converged solution in the step.

3.2.1. Elastic predictor
Trial values are calculated solving the elastic predictor problem:

$$\hat{\boldsymbol{\sigma}}^{trial}_{n+1} = \hat{\boldsymbol{\sigma}}^{trial}_n + \mathbf{D}^e(\hat{\boldsymbol{\sigma}}_{n+1})\Delta\boldsymbol{\varepsilon} \tag{23a}$$

$$\mathbf{q}^{trial}_{n+1} = \mathbf{q}_n + \Delta Sr\boldsymbol{\eta}(\hat{\boldsymbol{\sigma}}^{trial}_{n+1}, \mathbf{q}^{trial}_{n+1}(Sr_{n+1})). \tag{23b}$$

Eq. (23b) must be solved by iteration, and a suitable accurate procedure must be envisaged, as the accuracy of the elastic prediction affects significantly the final accuracy of the integration. If possible, a closed form evaluation of $\mathbf{q}^{trial}_{n+1}$ is strongly suggested, especially for large increments of the degree of saturation.

3.2.2. Plastic corrector
If $f^{trial}_{n+1} > 0$ the trial state lies outside the yield locus, and consistency needs to be restored. The trial state is the initial condition for the following system:

$$\begin{cases} \boldsymbol{\varepsilon}^e_{n+1} = (\boldsymbol{\varepsilon}^e_{n+1})^{trial} - \Delta\lambda\frac{\partial g}{\partial\hat{\boldsymbol{\sigma}}}\big|_{n+1} \\ \mathbf{q}_{n+1} = \mathbf{q}^{trial}_{n+1} + \Delta\lambda\mathbf{h}(\hat{\boldsymbol{\sigma}}_{n+1}, \mathbf{q}_{n+1}) \\ f(\hat{\boldsymbol{\sigma}}_{n+1}, \mathbf{q}_{n+1}) = 0 \end{cases}$$

where $(\boldsymbol{\varepsilon}^e_{n+1})^{trial} = \boldsymbol{\varepsilon}^e_n + \Delta\boldsymbol{\varepsilon}_{n+1}$ the unknowns are $\boldsymbol{\varepsilon}^e_{n+1}$, $\mathbf{q}_{n+1}$ and $\Delta\lambda$. The algebraic system (24) is non-linear and is solved via Newton's method.

4. Numerical implementation of the constitutive model

The two integration algorithms were implemented in a constitutive driver, in which the momentum balance, the water mass balance and the air mass balance are solved simultaneously at the representative elementary volume level. The transition between a two phase (saturated or dry) system and the general

Table 2
Parameters of the retention model.

Parameter	Main wetting	Main drying	Scanning
b	12	6.5	–
s_m^* (MPa)	2.4	6.7	–
n	1.34	1.34	–
m	0.254	0.254	.
s_{max} (MPa)	500	500	–
k_s (MPa^{-1})	–	–	0.02

Table 3
Mechanical parameters.

κ	G	λ	M	ξ	b_1	b_2	c_1
–	(MPa)	–	–	–	–	–	–
0.03	40	0.115	0.87	1.484	0.6	6.6	120

three-phase system is tackled with a physically based approach, by including water vapour and dissolved gas in the formulation [27].

4.1. Model equations

The hydro-mechanical model proposed by Romero and Jommi [29], which proved able to reproduce quite well a series of typical tests involving compacted clayey soils, is adopted in the following to describe the stress–strain behaviour of unsaturated soils. Basically, its formulation is an extension to unsaturated conditions of the mixed isotropic-rotational hardening model proposed by Dafalias [30] for saturated soils, adopting the average soil skeleton stress as constitutive stress. The relevant constitutive equations are summarised in Appendix A, for axisymmetric stress and strain paths only, adopting the usual geotechnical triaxial variables.

As for the retention domain, the model proposed by Della Vecchia et al. [31] was adopted. The model stems from the work of Romero and Vaunat [32], who evidenced the different mechanisms dominating water retention behaviour at the intra-aggregate and at the inter-aggregate structural levels in compacted clays. The conceptual model by Romero and Vaunat distinguishes between an intra-aggregate retention region, which is not affected by macroscopic void ratio, and an inter-aggregate one, depending on the void ratio through a linear scaling law. On this basis, Della Vecchia [33] and Romero et al. [34] proposed an enhanced retention model accounting for activity of the clay aggregates by means of an evolution law for the intra-aggregate void ratio, e_m.
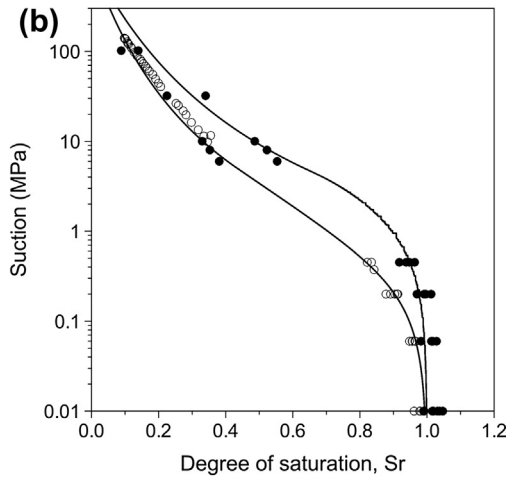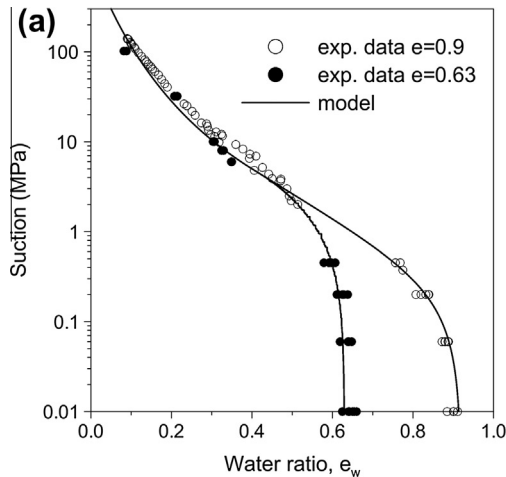

Fig. 3. Experimental results and numerical simulations for the volumetric strain along a wetting–drying–wetting path at constant net pressure.

Following [32], the portion of the water retention domain, which describes the retention mechanism of the inter-aggregate pore space, may be scaled in the range $e \geqslant e_w \geqslant e_m$. According to Della Vecchia et al. [31], e_m is continuously adjusted following the relationship:

$$e_m = e_m^* + \beta(e_w - e_m^*) \qquad \text{for } e_w > e_m^*, \tag{25}$$

where the parameter β quantifies the swelling and shrinking potential of the aggregates. Explicit introduction of the intra-aggregate void ratio e_m and of its evolution in the phenomenological retention equations characterises *multi-scale* interaction at the hydraulic level.

In the region bounded by the main drying and the main wetting curves, the hydraulic response of the material, i.e. the so called *scanning curves*, is assumed to be reversible. The constitutive equations of the hydraulic model are reported in Appendix A.

4.2. Parameter calibration

In the comparison presented in the following, the parameters of the adopted model were chosen in order to be in the representative range for Boom clay, from Romero and Jommi [29] for the mechanical part of the model, and Romero et al. [34] for the hydraulic one. The calibrated model parameters are summarised in Tables 2 and 3, while examples of the calibrated model performances are

Fig. 2. Main drying retention curves for the retention model at two void ratios, $e = 0.92$ and $e = 0.63$: (a) water ratio vs. suction, (b) degree of saturation vs. suction.
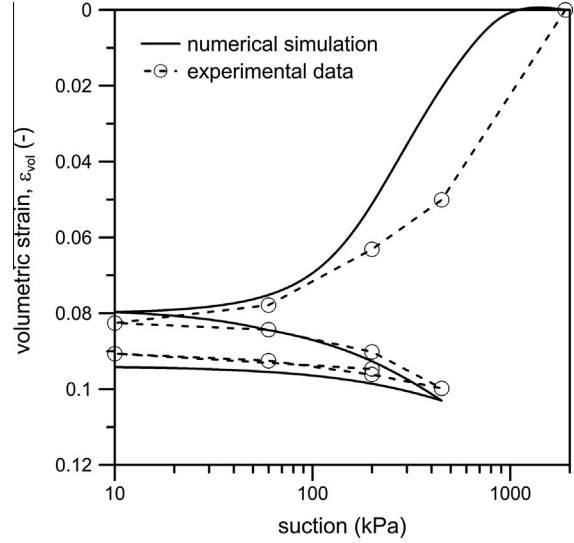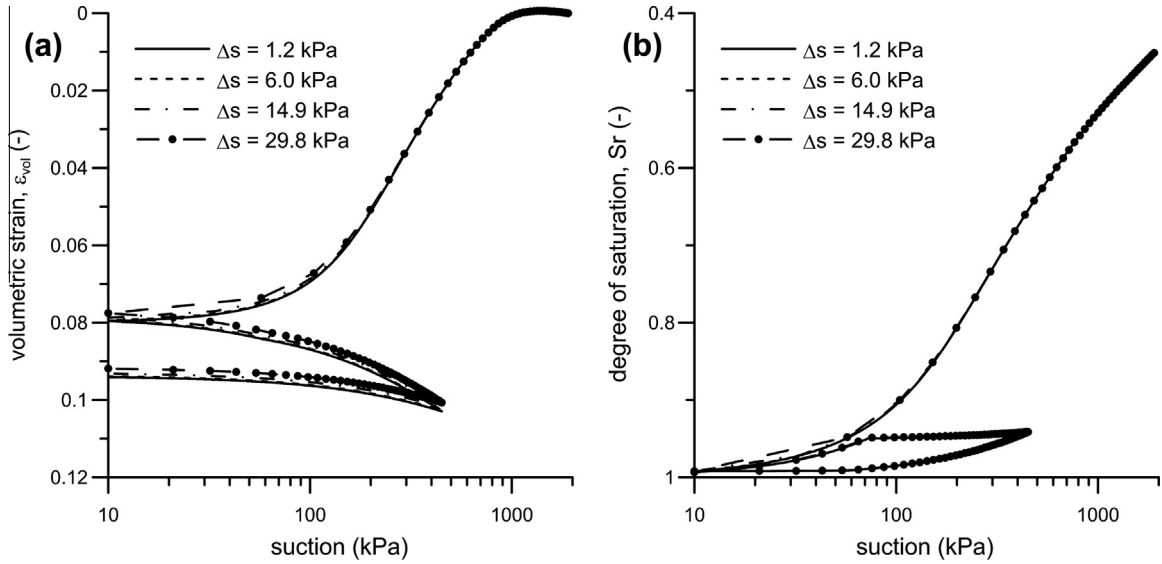
Fig. 4. Numerical solutions of the explicit algorithm with substepping for the evolution of volumetric strain and degree of saturation for the isotropic test, with steps of different size.
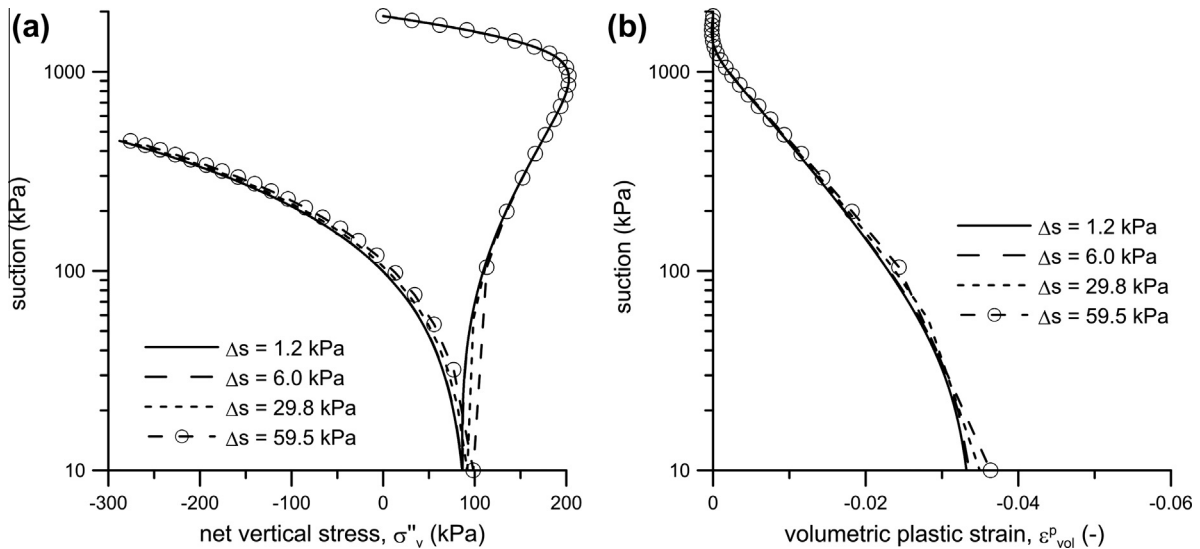

Fig. 5. Numerical solutions of the explicit algorithm with substepping for the evolution of vertical net stress and volumetric plastic strain for the isochoric test, obtained with steps of different size.

reported in Figs. 2 and 3. In Fig. 2, simulations of the main drying branches of the water retention domain for two different constant void ratios of $e = 0.90$ and $e = 0.63$ are reported. In Fig. 3, data are reported of volumetric strain experienced by a sample of Boom clay anisotropically compacted under unsaturated conditions and subjected to a wetting–drying–wetting cycle performed at constant applied isotropic net stress.

Material, sample preparation and experimental procedures of this and other tests may be found in [29,31], where the experimental data are discussed in more detail.

5. Evaluation of the performance of the algorithms

The simulations presented in the following are aimed at evaluating the performance of the explicit and implicit algorithms. To this aim, paradigmatic loading paths were considered, involving hydromechanical coupling and different kinematic conditions.

The tests refer to samples of Boom clay initially prepared by compaction in oedometer, on the dry side of the optimum Proctor, at a water content of $w = 0.15$ and at a dry density of $\rho_d = 1.37$ Mg/m^3. Oedometer compaction gave the soil an anisotropic structure, described by an initial surface rotated with respect to the hydro-static axis. The three paths analysed in the following describe:

- *Isotropic test*: wetting–drying–wetting cycle of a sample mounted in a controlled suction triaxial cell and previously compressed to an isotropic external confining stress $p = 600$ kPa.
- *Isochoric test*: wetting in a cell which prevents volumetric strain of an as-compacted sample.
- *Constant water content test*: isotropic compression of a sample previously brought to a water content of $w = 0.17$ after compaction by means of vapour transfer technique.

Details on experimental results of the three tests can be found in Romero [35] and Della Vecchia [33]. These three tests have been
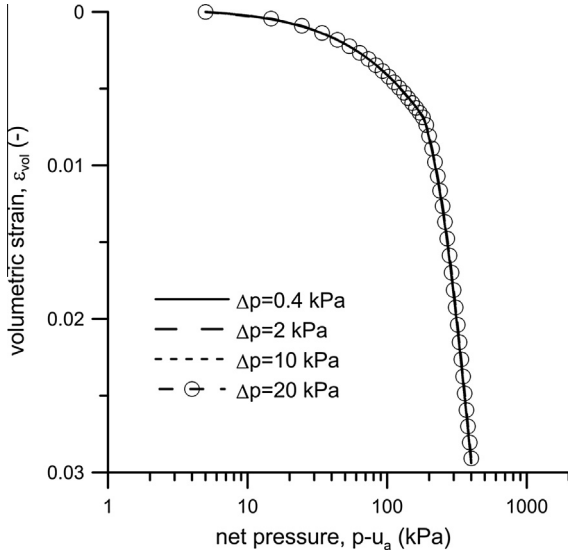
Fig. 6. Numerical solutions for the evolution of volumetric strain along the isotropic compression path at constant water content, obtained with steps of different size.

chosen to cover several aspects of hydromechanical coupling, including plastic deformation due to either suction variations at constant stress, suction variations at constant volume or net stress variations at constant water content. The paths chosen allow also to cover different external control conditions, including stress controlled and kinematically controlled tests, with imposed suction or water content. To evaluate the performance of the two algorithms, a set of analyses was performed on an Intel® Core™2 Duo processor (E7200 at 2.53 GHz). The *reference* numerical solutions were obtained by either the explicit or the implicit algorithm subdividing the whole stress paths in a huge number of steps (of the order of 10,000 for both algorithms) with an error tolerance of 10^{-9} (Eq. (20)). (see Fig. 4).

5.1. Explicit algorithm

For the three tests introduced, the explicit algorithm has been used to integrate the paths with a sequence of increments of increasing size. Fig. 4 a and b shows the performance of the explicit algorithm in the $\varepsilon_{vol} - s$ and $Sr - s$ planes with respect to the

simulation of the isotropic test. The tolerance used to perform these analysis was set equal to 10^{-5}. Thanks to the substepping procedure, the algorithm is always convergent, although inaccuracies arise during the integration of the first wetting path, for large initial step size in terms of Δs. The effectiveness of the substepping procedure is demonstrated by the fact that, independently from the Δs initially chosen, the total number of substeps needed for the integration of the whole path where plastic strains are involved is approximately the same for each simulation. As expected, no inaccuracy issues arise in the $Sr - s$ plane. In fact, as described in Section 3, the degree of saturation increment is calculated before entering the mechanical constitutive law routine as a function of the increments of suction and void ratio.

The results of the simulations for the isochoric test are shown in Fig. 5a and b. The algorithm proved to be very efficient, although some inaccuracies are evidenced for increasing integration step size both in terms of net vertical stress and, more significantly, in terms of volumetric plastic strains. Also in this case the total number of substeps required for the integration of the whole plastic path was found to be independent from the initial integration step size chosen.

The results are in accordance to those of Solowsky and Gallipoli [8], who have shown that the absolute error tends to grow as the integration step size increases. However, some inaccuracy may also be related to a detail of the strategy used to extend the substepping algorithm to the class of constitutive model for unsaturated soils considered in the paper. During the substepping procedure, the same reduction ΔT is applied to both $\Delta \varepsilon$ and ΔSr (Eq. (19)), following the criterion proposed in Eq. (21). A possible alternative would be to apply the reduction ΔT to the suction increment Δs, hence recalculating the corresponding ΔSr at each substep.

No appreciable error can be noticed in the numerical simulation of the constant water content test, presented in Fig. 6 in terms of evolution of volumetric strain with net average stress $p'':=p - u_a$, irrespective of the size of the integration step.

The different performance of the explicit algorithm along the hydromechanical paths analysed, may be preliminary evaluated with reference to the evolution of plastic volumetric strain as a function of degree of saturation (Fig. 7a) and of net vertical stress (Fig. 7b). A sub-vertical path in the $\varepsilon_{vol}^p - Sr$ plane implies that plastic strain develops mainly due to variations of mechanical conditions, as well as a sub-vertical path in the $\varepsilon_{vol}^p - \sigma_v''$ plane
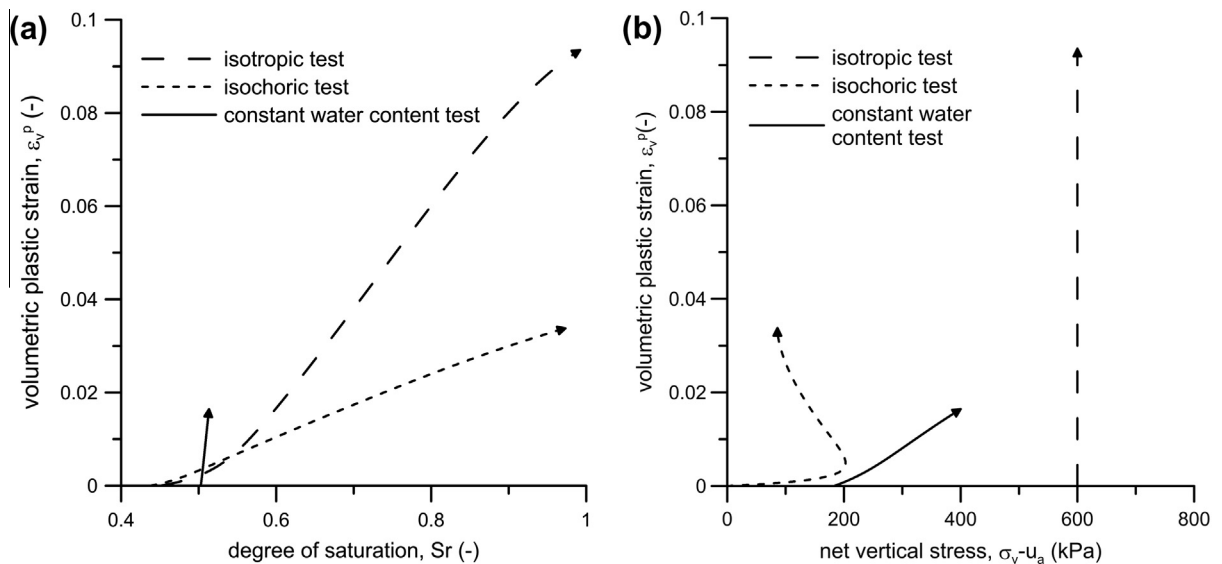

Fig. 7. Evolution of volumetric plastic strain along the hydro-mechanical paths.
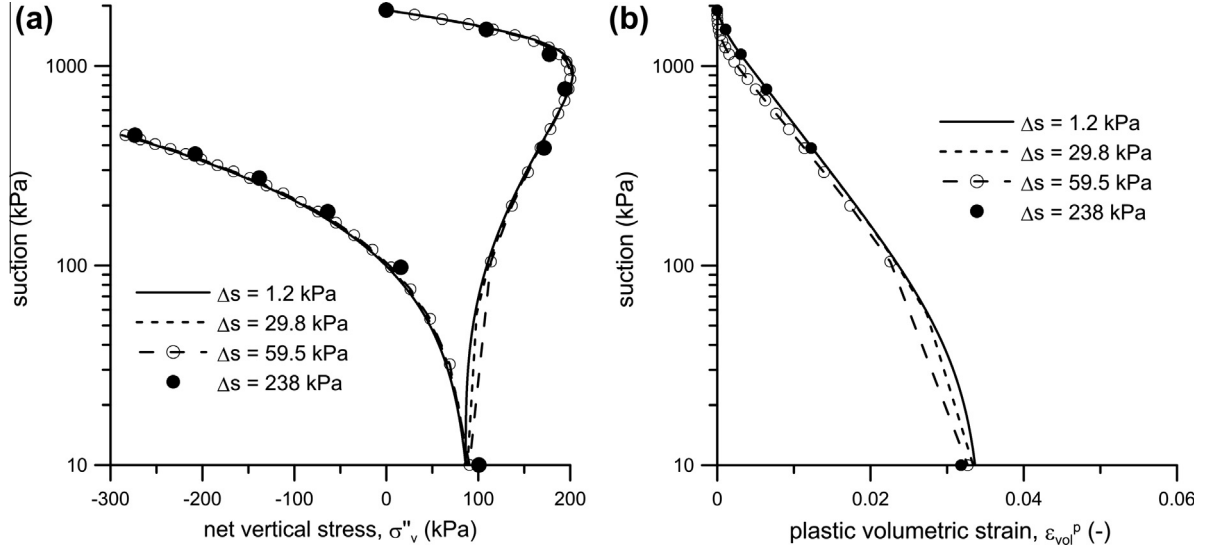
Fig. 8. Numerical solutions of the implicit algorithm for the evolution of vertical net stress and volumetric plastic strain along the isochoric test, obtained with different integration step size.
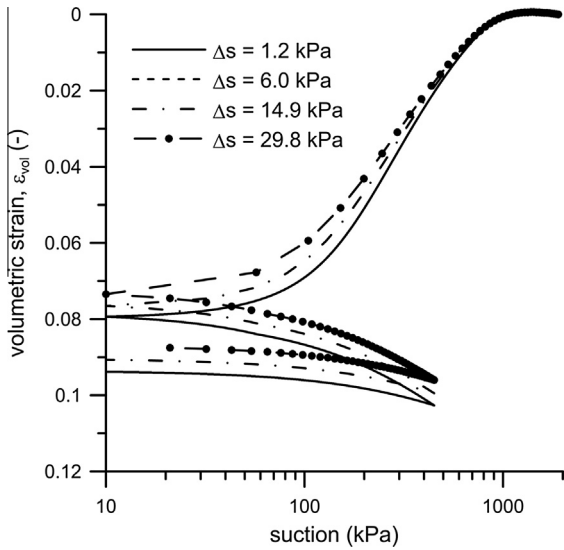

Fig. 9. Numerical solutions of the implicit algorithm for the evolution of volumetric strain along the wetting–drying–wetting of the isotropic test, obtained with different integration step size.

indicates that plastic strain takes place mainly due to changes in water content. The comparison between these three tests suggests that the accuracy is a function also of the hydro-mechanical path followed. Integration of paths along which plastic strains are induced by variations of the hydraulic conditions (e.g. the controlled suction isotropic test) appears to be more challenging from the numerical point of view. Viceversa, when volumetric plastic strain is mainly a consequence of mechanical loading (e.g. the constant water content test), the performance of the algorithm increases.

5.2. Implicit algorithm

Results of the parametric analyses performed on the isochoric test for the implicit algorithms are reported in Fig. 8, performed also with Δs = 60 kPa and 238 kPa. The implicit algorithm proved to be unconditionally stable and a reliable solution was obtained also with large integration step size, both in terms of net stress and plastic strain evolution. All the analyses presented in this sec-
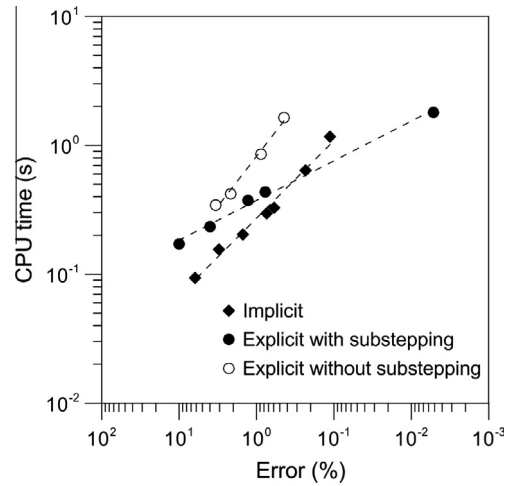

Fig. 10. Isochoric test: integration error vs. CPU time.

tion were performed expressing the dependence of the internal variables on the degree of saturation in a closed form.

Also in this case the performance of the algorithm is dependent on the hydro-mechanical path followed by the test. A clear example is shown in Fig. 9, where a decrease in accuracy for increasing integration step size is evidenced in terms of calculated volumetric strain during the isotropic test.

6. Performance and accuracy

Performance of the algorithms can be discussed, as a first approach, in terms of CPU time as a function of the error. Results for the isochoric suction controlled test are shown in Fig. 10. The error is computed with reference to the values of the stresses (as in Eq. (26)) at the end of the whole cyclic loading path:

$$e = \frac{\|\hat{\boldsymbol{\sigma}} - \hat{\boldsymbol{\sigma}}_{exact}\|}{\|\hat{\boldsymbol{\sigma}}_{exact}\|}. \tag{26}$$

For the sake of completeness, also the error obtained with an explicit algorithm without substepping is shown. The implicit algorithm and the explicit one without substepping show similar trends. As expected, lower CPU time is required by the implicit
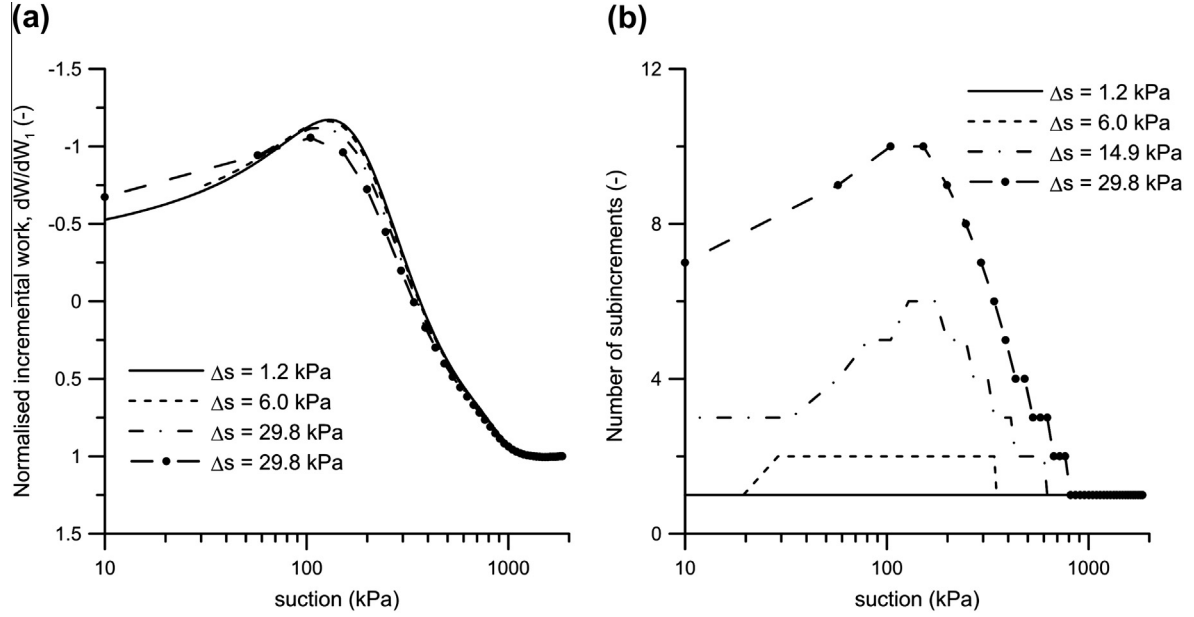
Fig. 11. Evolution of the performance of the explicit algorithm with substepping in the isotropic test. (a) Evolution of the normalised in-cremental work per unit volume with suction, (b) Number of substeps as a function of suction
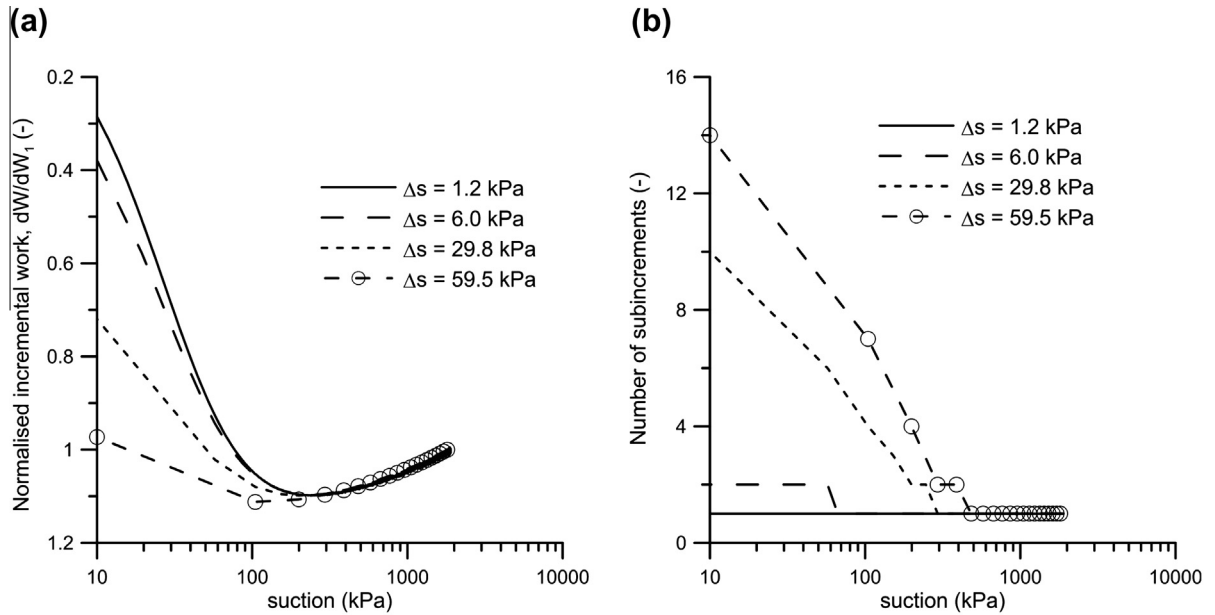

Fig. 12. Evolution of the performance of the explicit algorithm with substepping in the isochoric test. (a) Evolution of the normalised in-cremental work per unit volume with suction, (b) Number of substeps as a function of suction.

algorithm, thanks to its unconditional stability. The explicit algorithm with substepping is less efficient than the implicit one, unless when very low tolerances are imposed. In the latter case the explicit algorithm with substepping becomes competitive, although absolute CPU times increase beyond acceptable values in view of the numerical analysis of real scale problems. The trends confirm the results of Chaboche and Cailletaud [36], also in terms of higher convergence rate for the explicit algorithm with substepping.

Total CPU time, which increases with the number of substeps, is mostly attributable to specific time steps which appear to be particularly challenging in terms of convergence and accuracy. Gonzalez and Gens [19] have already observed that the number of substeps increases dramatically for high curvature of the stress path.

To provide a more objective criterion for identifying those time steps, in which convergence and accuracy issues may be encountered in general hydro-mechanical paths, the discretised incremental work per unit volume was analysed along the integration paths. According to Houlsby [37], the incremental work per unit volume, dW, may be written as

$$\mathrm{d}W = \hat{\boldsymbol{\sigma}} \cdot \mathrm{d}\boldsymbol{\varepsilon} - n(u_g - u_l)\,\mathrm{d}S_r \tag{27}$$

where n is porosity.

Fig. 11 shows the evolution with suction of both the normalised incremental work dW/dW_1 and the number of subincrements of each step. The normalising quantity dW_1 is defined as the incremental work corresponding to the first integration step. It can be
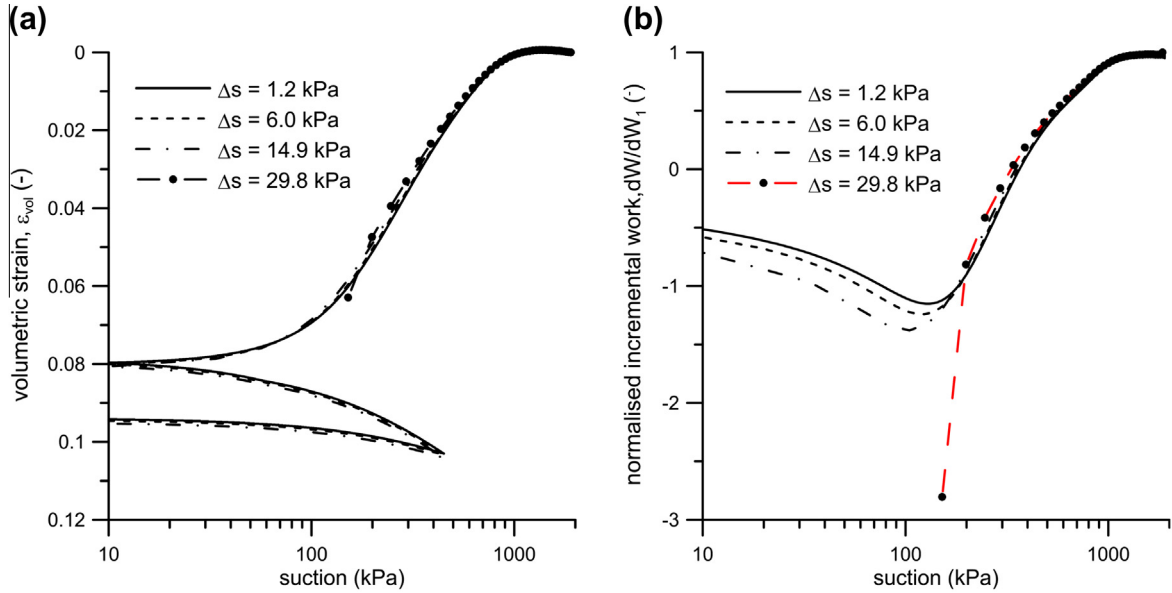
Fig. 13. Evolution of the incremental work per unit volume during the constant p'' test: algorithm without substepping. (a) Evolution of volumetric strain against suction, (b) Normalised incremental work evolution.
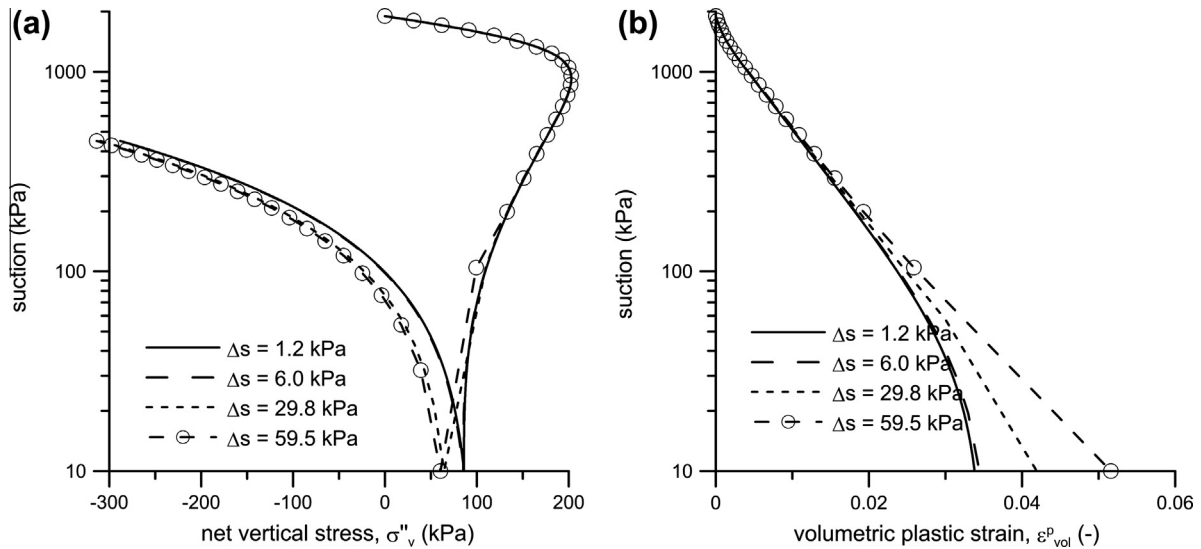

Fig. 14. Numerical solutions of the explicit algorithm without substepping for the evolution of vertical net stress and volumetric plastic strain along the wetting–drying cycle at constant volume, obtained with steps of different size.

observed that the number of subincrements required by the substepping procedure increases as the rate of normalised incremental work with the external controlling variable (i.e. suction in this case) decreases. In particular, the maximum number of substeps corresponds to a minimum in terms of normalised incremental work.

An identical behaviour is shown by the algorithm in the isochoric test (Fig. 12). The number of substeps increases as the normalised incremental work decreases, and reaches its maximum value when dW/dW_1 is minimum.

To further investigate the link between increasing convergence and accuracy issues of the algorithms and the gradient of the incremental work per unit volume, the isotropic test has been simulated again with the explicit algorithm but without substepping. Substepping has been inhibited by setting a high value of tolerance TOL (see Section 3.1.3). The numerical simulations confirm that the refined explicit algorithm without substepping is rather effi-

cient, although only conditionally stable. If the given integration step is too large, the algorithm diverges as shown in Fig. 13a for a step size $\Delta s = 29.8$ kPa. The onset of loss of accuracy seems to correspond to a stationary point in dW. When the step size is too large, the explicit algorithm without substepping is no longer able to converge.

On the contrary, no convergence problems were found in the numerical simulation of the isochoric test, even using the algorithm without substepping and a larger step size with $\Delta s = 59.5$ kPa. Results in terms of evolution of net vertical stress $\sigma_v'' = \sigma_v - u_a$ against suction are presented in Fig. 14a. Nevertheless, although in this plane no relevant accuracy problems occur (even for the simulation with suction integration step of 59.5 kPa), the prediction in terms of volumetric plastic strain (Fig. 14b) shows large errors. It is worth noting that inaccuracies start to be evident for a value of suction $s = 200$ kPa, which again corresponds to the maximum of nor-

malised incremental work (Fig. 12a). When dW/dW$_1$ starts to decrease, explicit integration issues increase.

7. Conclusions

Formulations proposed to model the constitutive behaviour of unsaturated soils based on generalised stress definitions, including both degree of saturation and suction in the definition of the constitutive variables, are characterised by strong non linearities due to hydromechanical coupling. As a consequence, refined algorithms are mandatory for their numerical implementation in finite element codes. A refined Runge–Kutta–Dormand–Prince explicit algorithm with automatic substepping and a fully implicit Euler scheme were tested to this aim, on an elastoplastic constitutive model with generalised hardening. Both explicit and implicit procedures proved to be rather efficient in the integration of the hydromechanical laws at the Gauss point level. The implicit algorithm is not only unconditionally stable, but also rather accurate. The explicit algorithm with substepping is rather efficient, and becomes competitive with the implicit one when very small errors can be tolerated. Nonetheless, in view of the implementation in numerical codes for the analysis of real scale problems, the implicit algorithm is advantageous for affordable CPU times. In spite of convergence, accuracy issues arise along selected hydromechanical paths.

An attempt was made to pick up a suitable indicator of the possible onset of accuracy issues. The discretised incremental hydromechanical work per unit volume, following the theoretical definition given by Houslby [37], was calculated along the paths analysed. The quantity was then normalised with its estimation at the first step. It was observed that plotting the evolution of this scalar variable as a function of the pertinent static or kinematic variables helps in identifying the first appearance of accuracy problems. In particular, the onset of loss of convergence for the explicit approach without substepping and of accuracy for both the explicit and the implicit algorithms was found to be linked with points of stationarity of dW. As soon as a minimum of dW is approached, the explicit algorithm solution starts to be significantly influenced by the size of the step. As a consequence, the algorithm without substepping might not be able to converge, depending on the controlling kinematic and static variables, and an increasing number of substeps is required by the adaptive algorithm to met the fixed tolerance. Also, the implicit algorithm may loose accuracy when a stationary point in the incremental work is approached. As the convergence and accuracy issues are reduced with the step size, discretised normalised incremental work may be possibly exploited as useful aid in adaptive time stepping algorithms.

8. Acknowledgments

Appendix A. Model equations

The model adopted for the simulation of the coupled hydromechanical behaviour of unsaturated soils is a combination of the mechanical laws proposed by Romero and Jommi [29] and the retention curve proposed by Della Vecchia [33] (see also Della Vecchia et al. [31]). The readers may refer to the original references for a detailed discussion of the models equations and of the relevant calibration procedures. A brief summary of the model's equations is reported here, with reference to axisymmetric stress and strain paths.

The elastic behaviour is described by

$$\dot{\hat{p}} = \frac{1+e}{\kappa} \hat{p} \dot{\varepsilon}_{vol}, \qquad \dot{q} = 3G\dot{\varepsilon}_d, \tag{A.1}$$

where $\hat{p}$ and q are the isotropic and deviator stresses in axisymmetric conditions and ε_{vol} and ε_d the corresponding work-conjugate variables. The yield function,

$$f = (q - M_\alpha \hat{p})^2 + \left(M^2 - M_\alpha^2\right)\hat{p}(\hat{p} - \hat{p}_c) = 0, \tag{A.2}$$

depends on two internal variables, $\hat{p}_c$ and M_α, ruling isotropic and rotational hardening, respectively. M represents the slope of the critical state line in the $q - \hat{p}$ plane. An associated flow rule is adopted to describe plastic strain direction ($f = g$). The preconsolidation stress $\hat{p}_c$ is assumed to be a function of the degree of saturation and of the preconsolidation pressure in saturated conditions p_c^{sat} as

$$\hat{p}_c = p_c^{sat}(1 - b_1(1 - e^{b_2(1-Sr)})), \tag{A.3}$$

where b_1 and b_2 are model parameters.

To express the evolution of the internal variables with plastic strains, the classical Cam-clay volumetric hardening law was chosen for the evolution of p_c^{sat},

$$\dot{p}_c^{sat} = \frac{1+e}{\lambda - \kappa} p_c^{sat} \dot{\varepsilon}_{vol}^p, \tag{A.4}$$

where λ is the slope of the NCL.

Rotational hardening is assumed to be governed by the difference between the current obliquity $q/\hat{p}$ and the current inclination M_α of the yield surface:

$$\dot{M}_\alpha = c_1(q/\hat{p} - \zeta M_\alpha)|\dot{\varepsilon}_{vol}^p|, \tag{A.5}$$

where c_1 and ζ are model parameters ruling the rotation rate and the limiting rotation, respectively.

The retention model is based on the conceptual subdivision between intra–aggregate and inter–aggregate pores. The model distinguishes between an intra–aggregate retention region, which is not affected by void ratio, and an inter–aggregate one, depending on the void ratio through a linear scaling law, accounting explicitly for activity of the clay aggregates. Assuming that void ratio does not influence the intra–aggregate retention mechanisms, the intra–aggregate portion of the retention domain is delimited by main wetting and main drying branches, uniquely linking the suction to a measure of water content. Each branch may be given the expression

$$e_w = \frac{be_m^*}{\ln\left(\frac{s_{max}}{s_m^*}\right)}\left[\frac{b + \ln\left(\frac{s_{max}}{s_m^*}\right)}{b + \ln\left(\frac{s}{s_m^*}\right)} - 1\right] \qquad \text{for } s < s_m^*. \tag{A.6}$$

In the previous equation, e_w is the water ratio on the drying or the wetting branch of the curve, s_{max} is the maximum suction attainable, corresponding to the value of s for $e_w = 0$, s_m^* are the suction values corresponding to e_{wm}^*, i.e. the smallest value of water ratio corresponding to saturated micro-voids and empty macro-voids. Parameter b is related to the average slope of the relevant curve in this region.

The portion of the water retention domain, which describes the retention mechanism of the inter–aggregate pore space, may be scaled in the range $e \geqslant e_w \geqslant e_m$ with the expression:

$$e_w = e_m + (e - e_m)\left[1 - \frac{\ln\left(1 + \frac{s}{s_m}\right)}{2}\right]\left[\frac{1}{1 + (\alpha s)^n}\right]^m \qquad \text{for } s > s_m^*, \tag{A.7}$$

where m and n are model parameters. Microscopic void ratio e_m is continuously adjusted following the relationship:

$$e_m = e_m^* + \beta\left(e_w - e_m^*\right) \qquad \text{for } e_w > e_m^*, \qquad (A.8)$$

where the parameter β describes the slope of the approximating linear interpolation of e_m for $e_w > e_{wm}^*$ and quantifies the swelling and shrinking potential of the aggregates.

The variable s_m is assumed to change following the microscopic portion of the relevant branch of the water retention domain:

$$s_m = s_m^* \exp\left[\frac{be_m^*\left(b + \ln\left(\frac{s_{max}}{s_m^*}\right)\right)}{e_{wm}\ln\left(\frac{s_{max}}{s_m^*}\right) + be_m^*} - b\right]. \qquad (A.9)$$

In the region bounded by the main drying and the main wetting curves, the hydraulic response of the material is assumed to be reversible. A linear relationship is postulated between degree of saturation and suction:

$$\mathrm{d}S_r = -k_s \mathrm{d}s, \qquad (A.10)$$

where k_s is a constant parameter of the model.

References

[1] Sloan SW. Substepping schemes for the numerical integration of elastoplastic stress–strain relations. Int J Numer Methods Eng 1987;24(5):893–911. http://dx.doi.org/10.1002/nme.1620240505.

[2] Sloan SW, Abbo AJ, Sheng D. Refined explicit integration of elastoplastic models with automatic error controls. Eng Comput 2001;18(1/2):121–94. http://dx.doi.org/10.1108/02644400110365842.

[3] Sheng D, Sloan SW, Gens A, Smith DW. Finite element formulation and algorithms for unsaturated soils. Part I: Theory. Int J Numer Anal Methods Geomech 2003;27:745–65. http://dx.doi.org/10.1002/nag.295.

[4] Sheng D, Smith DW, Sloan SW, Gens A. Finite element formulation and algorithms for unsaturated soils. Part II: Verification and application. Int J Numer Anal Methods Geomech 2003;27(9):767–90.

[5] Sheng D, Sloan SW, Gens A. A constitutive model for unsaturated soils: thermomechanical and computational aspects. Comput Mech 2004;33(6):453–65.

[6] Sheng D, Gens A, Fredlund DG, Sloan SW. Unsaturated soils: from constitutive modelling to numerical algorithms. Comput Geotech 2008;35(6):810–24.

[7] Sánchez M, Gens A, Guimarães L, Olivella S. Implementation algorithm of a generalised plasticity model for swelling clays. Comput Geotech 2008;35(6):860–71.

[8] Solowski WT, Gallipoli D. Explicit stress integration with error control for the barcelona basic model. Part II: Algorithms efficiency and accuracy. Comput Geotech 2010;37(1–2):68–81. http://dx.doi.org/10.1016/j.compgeo.2009.07.003.

[9] Solowski WT, Gallipoli D. Explicit stress integration with error control for the barcelona basic model: Part I: Algorithms formulations. Comput Geotech 2010;37(1–2):59–67. http://dx.doi.org/10.1016/j.compgeo.2009.07.004.

[10] Solowski WT, Sheng D, Sloan SW. Explicit stress integration with reduced drift for barcelona basic model. In: Alonso E, Gens A, editors. Unsaturated soils: proceedings of the fifth international conference on unsaturated soils. Barcelona, vol. 2. London: Taylor & Francis Group; 2011. p. 1075–80.

[11] Vaunat J, Cante JC, Ledesma A, Gens A. A stress point algorithm for an elastoplastic model in unsaturated soils. Int J Plast 2000;16(2):121–41.

[12] Zhang H, Heeres O, de Borst R, Schrefler B. Implicit integration of a generalized plasticity constitutive model for partially saturated soil. Eng Comput 2001;18(1/2):314–36.

[13] Hoyos LR, Arduino P. Implicit algorithm for modeling unsaturated soil response in three-invariant stress space. Int J Geomech 2008;8(4):266–73.

[14] Zhang HW, Zhou L. Implicit integration of a chemo-plastic constitutive model for partially saturated soils. Int J Numer Anal Meth Geomech 2008;32(14):1715–35.

[15] Tamagnini R, De Gennaro V. Implicit integration of an axtended cam clay model for unsaturated soils. In: Toll DG, Augarde CE, Gallipoli D, Wheeler SJ, editors. Advances in geo-egineering, proc 1st European conference on unsaturated soils, Durham (UK), 2–4th July; 2008. p. 713–9.

[16] Potts D, Ganendra DM. An evaluation of substepping and implicit stress point algorithms. Comput Methods Appl Mech Eng 1994;119(3–4):341–64.

[17] Abbo S, Sloan AJ. An automatic load stepping algorithm with error control. Int J Num Methods Eng 1996;39(10):1737–59.

[18] Hofmann M, Hofstetter G, Ostermann A. Comparison of stress update algorithms for partially saturated soil models. In: Benz T, Nordal S, editors. Numerical methods in geotechnical engineering; 2010. p. 325–30.

[19] González NA, Gens A. Evaluation of a constitutive model for unsaturated soils: stress variables and numerical implementation. In: Alonso E, Gens A, editors. Unsaturated soils: proceedings of the fifth international conference of unsaturated soils, Barcelona, vol. 2. Taylor & Francis Group; 2011. p. 829–35.

[20] Nuth M, Laloui L. Effective stress concept in unsaturated soils: clarification and validation of a unified framework. Int J Numer Anal Methods Geomech 2008;32:771–801.

[21] Jommi C. Remarks on the constitutive modelling of unsaturated soils. In: Tarantino A, Mancuso C, editors. Experimental evidence and theoretical approaches in unsaturated soils, Balkema, Rotterdam; 2000. p. 139–53.

[22] Jakobsen KP, Lade PV. Implementation algorithm for a single hardening constitutive model for frictional materials. Int J Numer Anal Methods Geomech 2002;26(7):661–81. http://dx.doi.org/10.1002/nag.217.

[23] Borja RI, Lee SR. Cam-clay plasticity. Part I: Implicit integration of elasto-plastic constitutive relations. Comput Methods Appl Mech Eng 1990;78(1):49–72.

[24] Tamagnini C, Castellanza R, Nova R. A generalized backward Euler algorithm for the numerical integration of an isotropic hardening elastoplastic model for mechanical and chemical degradation of bonded geomaterials. Int J Numer Anal Methods Geomech 2002;26(10):963–1004. http://dx.doi.org/10.1002/nag.231.

[25] Borja RI. Cam-clay plasticity. Part V: A mathematical framework for three-phase deformation and strain localization analyses of partially saturated porous media. Comput Methods Appl Mech Eng 2004;193(48–51):5301–38.

[26] Ortiz M, Popov EP. Accuracy and stability of integration algorithms for elastoplastic constitutive relations. Int J Numer Methods Eng 1985;21(9):1561–76. http://dx.doi.org/10.1002/nme.1620210902.

[27] Cattaneo F, Della Vecchia G, Jommi C. A driver for the integration of coupled hydro-mechanical constitutive laws for unsaturated soils. In: Alonso E, Gens A, editors. Unsaturated soils: proceedings of the fifth international conference on unsaturated soils. Barcelona, vol. 2. London: Taylor & Francis Group; 2011. p. 1017–23.

[28] Quarteroni A, Sacco R, Saleri F. Numerical mathematics. second ed. Springer; 2007.

[29] Romero E, Jommi C. An insight into the role of hydraulic history on the volume changes of anisotropic clayey soils. Water Resour Res 2008;44. http://dx.doi.org/10.1029/2007WR006558.

[30] Dafalias YF. An anisotropic critical state soil plasticity model. Mech Res Commun 1987;13(6):341–7.

[31] Della Vecchia G, Jommi C, Romero E. A fully coupled elastic–plastic hydromechanical model for compacted soils accounting for clay activity. Int J Numer Anal Meth Geomech 2013;37(5):503–35. http://dx.doi.org/10.1002/nag.1116.

[32] Romero E, Vaunat J. Retention curves of deformable soils. In: Tarantino A, Mancuso C, editors. Experimental evidence and theoretical approaches in unsaturated soils, Balkema, Rotterdam; 2000. p. 91–106.

[33] Della Vecchia G. Coupled hydro-mechanical behaviour of compacted clayey soils. PhD thesis, Politecnico di Milano; 2009.

[34] Romero E, Della Vecchia G, Jommi C. An insight into the water retention properties of compacted clayey soils. Géotechnique 2011;61(4):313–28.

[35] E. Romero, Thermo-hydro-mechanical behaviour of unsaturated boom clay: an experimental study. PhD thesis, Universidad Politécnica de Catalunya, Barcelona, Spain; 1999.

[36] Chaboche JL, Cailletaud G. Integration methods for complex plastic constitutive equations. Comput Methods Appl Mech Eng 1996;133(1–2):125–55.

[37] Houlsby GT. The work input to an unsaturated granular material. Géotechnique 1997;47(1):193–6.